ACTA ASTRONOMICA
Vol. **68** (2018) pp. 159–181

CCD Photometry, Light Curve Modeling and Period Analysis of the Overcontact Eclipsing Binary BN Ari

K. B. Alton[1], R. H. Nelson[2,3] and D. R. S. Boyd[4]

[1] UnderOak Observatory, Cedar Knolls, NJ 07927, USA
e-mail: mail@underoakobservatory.com
[2] Mountain Ash Observatory, 1393 Garvin Street, Prince George, BC, V2M 3Z1, Canada
[3] Guest Investigator, Dominion Astrophysical Observatory, Herzberg Institute of Astrophysics, National Research Council of Canada
e-mail: bob.nelson@shaw.ca
[4] British Astronomical Association Variable Star Section
West Challow Observatory, 5 Silver Lane,, Wantage OX12 9TX, United Kingdom
e-mail: davidboyd@orion.me.uk

Received May 10, 2018

ABSTRACT

We present photometric and spectroscopic data of BN Ari, a totally eclipsing variable star. 15 new times-of-minimum have been determined. These along with other published eclipse timings were used to update the linear ephemeris and evaluate changes in orbital periodicity. Radial velocity data along with a definitive classification spectrum are reported for the first time. Simultaneous modeling of multicolor light curves and radial velocity data was accomplished using the Wilson-Devinney code with optimization by differential corrections. The weight of evidence from evaluating both the eclipse timing differences and light curve modeling indicates that BN Ari is most likely a triple system.

Key words: *binaries: eclipsing – binaries: close – Stars: individual: BN Ari*

1. Introduction

BN Ari (GSC 1761-1934) was first reported to be an overcontact W UMa-type binary system over 14 years ago. Except for times-of-minima and sparsely sampled survey data, no complete light curves for BN Ari had been published until 2015. The periodic variable behavior of BN Ari ($P = 0.299376$ d) was first reported by Otero *et al.* (2004) using data from the Northern Sky Variability Survey (Woźniak *et al.* 2004) and the All Sky Automated Survey (Pojmański *et al.* 2005). Thereafter, times-of-minimum light have been published at irregular intervals since 2007. More recently, this system was investigated by Michaels (2015) in which multicolor (*B, V, g', r'* and *i'*) photometry was used to determine its physical and geometric elements after light curve modeling. Here we further examine

sinusoidal-like variations in the orbital period that have become more apparent with additional eclipse timings along with providing definitive absolute parameters for BN Ari derived from Roche modeling with new radial velocity (RV) and stellar classification spectra.

2. Observations and Data Reduction

2.1. Photometry

CCD photometric sessions were conducted at UnderOak Observatory (UO) between November 18, 2016 and January 9, 2017. Automated imaging was performed with photometric *B, V* and I_c filters manufactured according to the Johnson-Cousins-Bessel prescription. Equipment included a focal reduced (f/6.4) 0.28-m catadioptic telescope with an SBIG ST-8XME CCD camera mounted at the Cassegrain focus. Image acquisition (raw light frames, darks, and flats), calibration, registration and astrometric plate solutions were performed as described elsewhere (Alton 2016). Exposure times varied according to bandpass ($B = 60$ s, $V = 45$ s, $I_c = 45$ s). Stellar magnitudes (MPOSC3, Warner 2007) and normalized flux (*B, V* and I_c) were calculated using a fixed ensemble of four non-varying comparison stars (Table 1) in the same field-of-view (FOV). CCD observations at Mountain Ash Observatory (MAO) located in Prince George, B.C., Canada were carried out from November 10, 2016 and December 8, 2016. The equipment included a 0.33-m f/4.5 Newtonian optical assembly on a Paramount ME mount (Software Bisque), and a SBIG ST-10XME CCD camera equipped with Custom Scientific *V, R*$_c$, and I_c filters. Automated filter changes and imaging were carried out using THESKY6 (ver. 6.0.0.65), CCDSOFT (ver. 5.00.210), and ORCHESTRATE (ver. 1.00.020) all by Software Bisque, Inc. Exposure times varied from 100–150 s (*V* filter),

T a b l e 1

Astrometric coordinates (J2000) and color indices ($B-V$) for BN Ari and an ensemble of four comparison stars used for photometric reduction of data at UO

Star Identification	R.A.	Dec.	MPOSC3[(a)] ($B-V$)
BN Ari	$02^h09^m07\overset{s}{.}78$	$26°29'07\overset{''}{.}1$	0.978
TYC 1761-2324-1	$02^h10^m35\overset{s}{.}55$	$26°32'07\overset{''}{.}3$	0.956
GSC 1761-1732	$02^h10^m05\overset{s}{.}89$	$26°26'44\overset{''}{.}4$	0.496
TYC 1761-2281-1	$02^h09^m28\overset{s}{.}81$	$26°22'29\overset{''}{.}9$	0.598
GSC 1761-1582	$02^h10^m18\overset{s}{.}06$	$26°30'54\overset{''}{.}5$	0.552

(a) MPOSC3 is a hybrid catalog (Warner 2007) which includes a large subset of the Carlsberg Meridian Catalog (CMC-14) as well as data from the Sloan Digital Sky Survey (SDSS).

T a b l e 2

Astrometric coordinates (J2000) and color indices ($B-V$) for BN Ari and the comparison and the check stars used for photometric reduction of data at MAO

	Star Identification	R.A.	Dec.	SIMBAD ($B-V$)
Variable	BN Ari	$02^h09^m07\overset{s}{.}78$	$26°29'07\overset{''}{.}11$	0.81
Comparison	GSC 1761-2282	$02^h09^m46\overset{s}{.}94$	$26°22'05\overset{''}{.}12$	1.09
Check	GSC 1761-1336	$02^h07^m58\overset{s}{.}83$	$26°17'31\overset{''}{.}24$	0.52
Check	GSC 1761-1592	$02^h09^m53\overset{s}{.}54$	$26°12'18\overset{''}{.}91$	0.26

60–90 s (R_c), and 170–220 s (I_c). The computer clock was updated automatically immediately prior to each session using one of the Windows time servers. Image reduction was performed with Mira v7.9986 UE (Mirametrics Inc.) and consisted of the usual bias, dark, flat-field corrections for aperture photometry. Differential comparisons were obtained using the comparison and check stars listed in Table 2. In all cases, error due to differential refraction and color extinction was minimized by only using images taken above 30° altitude (at airmass < 2.0).

2.2. Light Curve Analysis

Simultaneous multicolor (B, V, R_c and I_c) light curve type modeling was performed with the programs WDWINT56A[1] and/or PHOEBE 0.31A (Prša and Zwitter 2005), both of which employ the Wilson-Devinney (W–D) code (Wilson and Devinney 1971, Wilson 1979, Wilson 1990). Once each model fit was finalized, spatial renderings of BN Ari were produced by BINARY MAKER 3 (Bradstreet and Steelman 2002). Times-of-minimum were calculated using the method of Kwee and van Woerden (1956).

2.3. Classification Spectrum

Spectra of BN Ari were recorded at West Challow Observatory (WCO) on October 27, 2017 and November 1, 2017 using a 0.28-m SCT (f/5.5) and a LISA spectrograph ($R \approx 1000$) coupled with a SXVR-H694 CCD camera. Five 300 s exposures were taken each night during a total primary eclipse when the primary star is completely obscured by its more massive but cooler companion. Although cooler ($\Delta T \approx 100$ K), the total luminosity of this system is dominated by the more massive star due to its 2.3-fold greater surface area. Raw spectral images were dark and bias subtracted, flat fielded, wavelength calibrated with an Ar/Ne lamp and corrected for atmospheric and instrument response using spectra of the nearby B5V Miles Library (Sánchez-Blázquez *et al.* 2006) star HD3369 taken before and after the

[1] *https://www.variablestarssouth.org/bob-nelson/*

spectra of BN Ari. The individual corrected and calibrated spectra of BN Ari were combined to yield a 1D spectral profile for each night. The spectra from both nights were very similar with the one on November 1, 2017 having a better signal to noise ratio of 73. This spectrum was dereddened with $E(B-V) = 0.006 \pm 0.001$ mag and visually compared to spectra from the Pickles Stellar Spectral Flux Library (Pickles 1998) to determine the closest fit.

2.4. Radial Velocity Determinations

A total of 17 medium resolution (mean $R \approx 10\,000$) spectra of BN Ari were acquired at the Dominion Astrophysical Observatory (DAO) in Victoria, British Columbia, Canada between September 14, 2016 and September 12, 2017. The instrument included a Cassegrain spectrograph with a grating (# 1800Yb. 1800 lines/mm) blazed at 5000 Å in the 21121 configuration. This spectrograph when installed on the 1.85-m "Plaskett" telescope yielded a reciprocal first order linear dispersion of 10 Å/mm that approximately covered a wavelength region between 5000 Å and 5260 Å. A detailed description of the spectrometer, software and procedures for data reduction are described elsewhere (Nelson 2010).

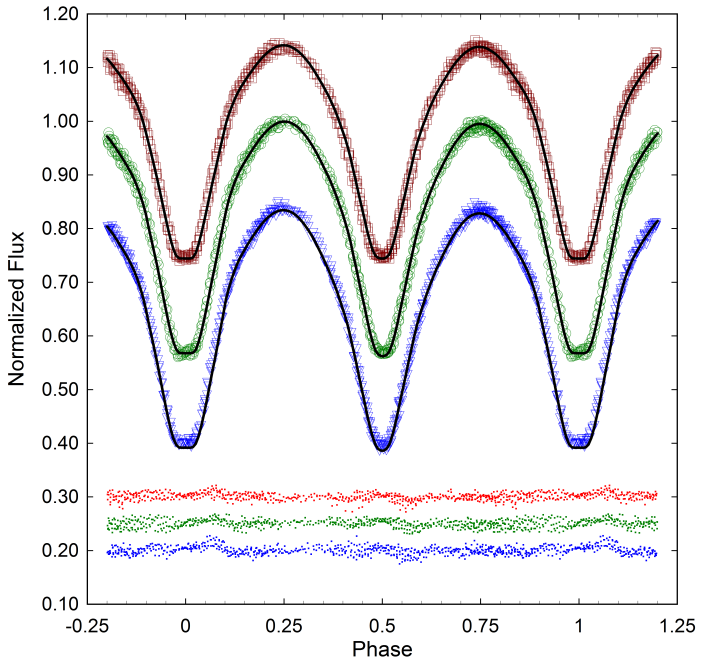

Fig. 1. Folded CCD light curves for BN Ari produced from photometric data obtained at UO between November 18, 2016 and January 9, 2017. The *top* (I_c), *middle* (V) and *bottom* curve (B) were reduced to normalized flux. Synthetic fits (solid-line) from Roche modeling assumed a W-type W UMa binary with a single hot spot. Flux and residuals from the model fits are offset for clarity.

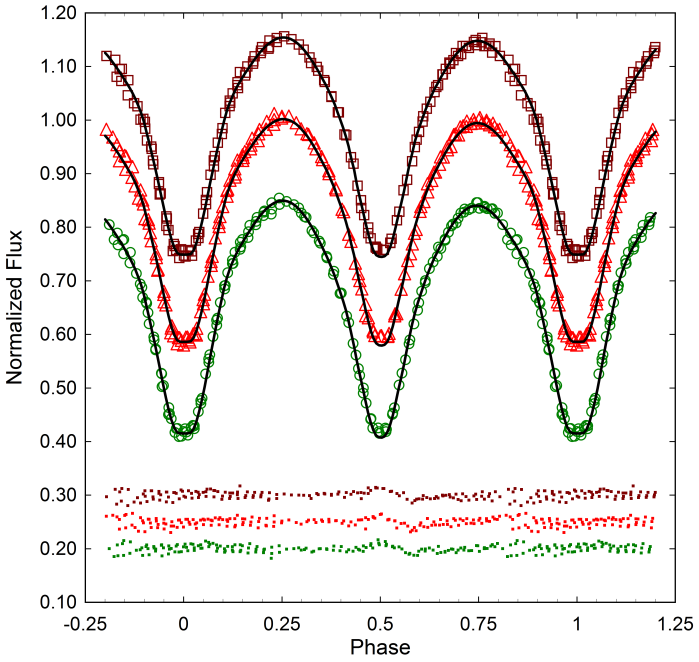

Fig. 2. Same as Fig. 1 for data obtained at MAO between November 10, 2016 and December 8, 2016.

3. Results and Discussion

3.1. Photometry

At UO, four comparison stars in the same FOV with BN Ari showed no remarkable variability over each imaging session and stayed within ± 0.006 mag for V and I_c filters and ± 0.009 mag for B passband (Table 1). Photometric values were used to derive normalized flux and catalog-based (MPOSC3) magnitudes with MPO Canopus. These results (B: $n = 572$, V: $n = 587$, and I_c: $n = 579$) yielded light curves that spanned 52 days between November 18, 2016 and January 9, 2017 (Fig. 1) and included nine new eclipse timings captured at minimum light. Reduction of instrumental magnitudes to normalized flux at MAO was similarly accomplished using differential aperture photometry. In this case a comparison and two check stars in the same FOV with BN Ari (Table 2) showed no remarkable variability over each imaging session. These data (V: $n = 156$, R_c: $n = 159$, and I_c: $n = 147$) produced another six eclipse timings at minimum light (Nelson 2017) and yielded period-folded light curves that spanned 28 days between November 10, 2016 and December 8, 2016 (Fig. 2). A final time-of-minimum was captured at WCO on August 29, 2017 as a prelude to producing the classification spectra.

3.2. Ephemerides

Light curve data collected at UO were period-folded after initially seeding the analysis with the orbital period (0.299376 d) reported by Otero *et al.* (2004), The Fourier routine (FALC, Harris *et al.* 1989) in MPO Canopus provided a slightly

shorter period solution (0.299361 ± 0.000001 d). Period determinations were independently assessed by applying periodic orthogonals (Schwarzenberg-Czerny 1996) to fit observations and analysis of variance (ANOVA) to evaluate fit quality In this case a comparable period solution at 0.299365 ± 0.000026 d was uniformly obtained for each bandpass (*B, V* and I_c). Light curve data acquired at MAO were similarly analyzed and resulted in an orbital period of 0.299376 ± 0.000056 d). A fourth and final period estimate (0.299374 ± 0.000006 d) was derived by folding ASAS survey data (Pojmański *et al.* 2005) captured between 2002 and 2009. New minima acquired at UO along with published values starting in 1999 (Table 3) were used to analyze eclipse timing differences (ETD) through 2017 when the latest times-of-minimum were reported. The reference epoch (Otero *et al.* 2004) employed for calculating difference between observed and predicted eclipse timings was defined by the following linear ephemeris for primary minimum:

$$\mathrm{HJD(MinI)} = 2\,451\,525.671 + 0.299376\,E\,. \qquad (1)$$

These differences are plotted against the period cycle number (Fig. 3) to visualize any potential changes in orbital period over time. Collectively the data are best fit by a parabolic relationship (Eq. 2) between ETD and time in the general form:

$$\mathrm{ETD}_{\mathrm{fitted}} = c_0 + c_1\,E + c_2\,E^2 + \tau\,. \qquad (2)$$

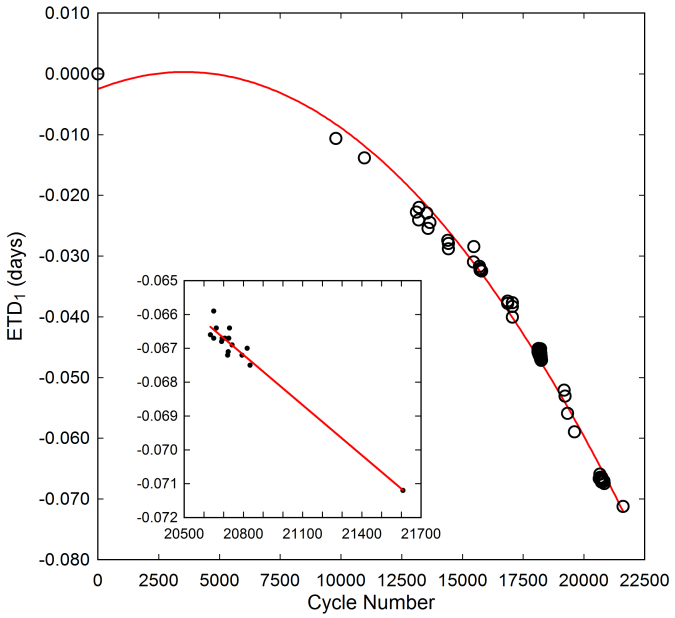

Fig. 3. Quadratic fit of eclipse timing differences for BN Ari between 1999 and 2017. Inset shows linear fit of the most recent (2016–2017) data.

T a b l e 3

Times-of-minimum and ETD for BN Ari used to calculate new ephemerides and perform LITE analysis

Times-of-minimum (HJD–2400000)	Cycle No.	ETD	Ref.	Times-of-minimum (HJD-2400000)	Cycle No.	ETD	Ref.
51525.6710	0	0.00000	1	56957.8025	18145	−0.04607	15
54456.2520	9789	−0.01066	2	56960.6468	18154.5	−0.04581	15
54805.3150	10955[(a)]	−0.02008	2	56960.7961	18155	−0.04619	15
54808.3150	10965	−0.01384	2	56962.5922	18161	−0.04635	15
55448.8210	13104.5	−0.02279	3	56962.7423	18161.5	−0.04594	15
55477.8592	13201.5	−0.02406	4	56962.8916	18162	−0.04635	15
55478.9091	13205	−0.02198	4	56970.6751	18188	−0.04656	15
55578.3010	13537	−0.02291	5	56970.8251	18188.5	−0.04629	15
55591.6207	13581.5	−0.02544	6	56971.7234	18191.5	−0.04614	15
55614.9730	13659.5	−0.02447	7	56978.3105	18213.5	−0.04528	16
55836.6580	14400	−0.02740	5	56978.4590	18214	−0.04646	16
55843.8416	14424	−0.02882	8	56980.7050	18221.5	−0.04577	15
55843.9922	14424.5	−0.02791	8	56980.8535	18222	−0.04698	15
56153.5439	15458.5	−0.03096	9	56981.6028	18224.5	−0.04607	15
56157.5880	15472	−0.02847	10	56985.6436	18238	−0.04692	15
56226.1419	15701	−0.03168	11	56985.7936	18238.5	−0.04662	15
56235.1228	15731	−0.03206	11	56987.5898	18244.5	−0.04664	15
56235.2722	15731.5	−0.03234	11	56988.6371	18248	−0.04719	15
56251.2887	15785	−0.03246	12	56988.7872	18248.5	−0.04672	15
56575.0589	16866.5	−0.03740	13	56989.8346	18252	−0.04711	15
56575.2082	16867	−0.03779	13	57270.7941	19190.5	−0.05206	15
56630.2929	17051	−0.03828	14	57278.7266	19217	−0.05304	15
56630.4432	17051.5	−0.03766	14	57310.0085	19321.5	−0.05588	17
56630.5905	17052	−0.04005	14	57395.6270	19607.5	−0.05892	18
56946.7258	18108	−0.04578	15	57702.6294	20633	−0.06661	19
56946.8760	18108.5	−0.04529	15	57707.5698	20649.5	−0.06591	19
56948.6721	18114.5	−0.04545	15	57707.7187	20650	−0.06670	19
56948.8215	18115	−0.04576	15	57728.6745	20720	−0.06722	19
56949.7196	18118	−0.04578	15	57729.5727	20723	−0.06715	19
56949.8696	18118.5	−0.04545	15	57730.6210	20726.5	−0.06666	19
56951.6657	18124.5	−0.04558	15	57711.6108	20663	−0.06644	20
56951.8153	18125	−0.04575	15	57719.5440	20689.5	−0.06680	20
56952.7133	18128	−0.04584	15	57720.5919	20693	−0.06670	20
56952.8633	18128.5	−0.04554	15	57724.6334	20706.5	−0.06674	20
56954.6594	18134.5	−0.04569	15	57731.5194	20729.5	−0.06644	20
56954.8087	18135	−0.04605	15	57735.5605	20743	−0.06692	20
56956.6058	18141	−0.04523	15	57750.5290	20793	−0.06717	20
56956.7551	18141.5	−0.04559	15	57758.4626	20819.5	−0.06705	20
56956.9043	18142	−0.04611	15	57762.6534	20833.5	−0.06746	20
56957.6533	18144.5	−0.04557	15	57994.5164	21608	−0.07122	20

(a) outlier removed from analysis

1. Otero *et al.* (2004) 2. Paschke (2009), 3. Nelson (2011), 4. Diethelm (2011), 5. Paschke (2011), 6. Nelson (2012), 7. Nagai (2012), 8. Diethelm (2012), 9. Hoňková *et al.* (2013), 10. Paschke (2013), 11. Nagai (2013), 12. Hübscher and Lehmann (2013), 13. Nagai (2014), 14. Hübscher (2014), 15. Michaels (2015), 16. Hübscher (2015), 17. Nagai (2016), 18. Samolyk (2016), 19. Nelson (2017), 20. This paper.

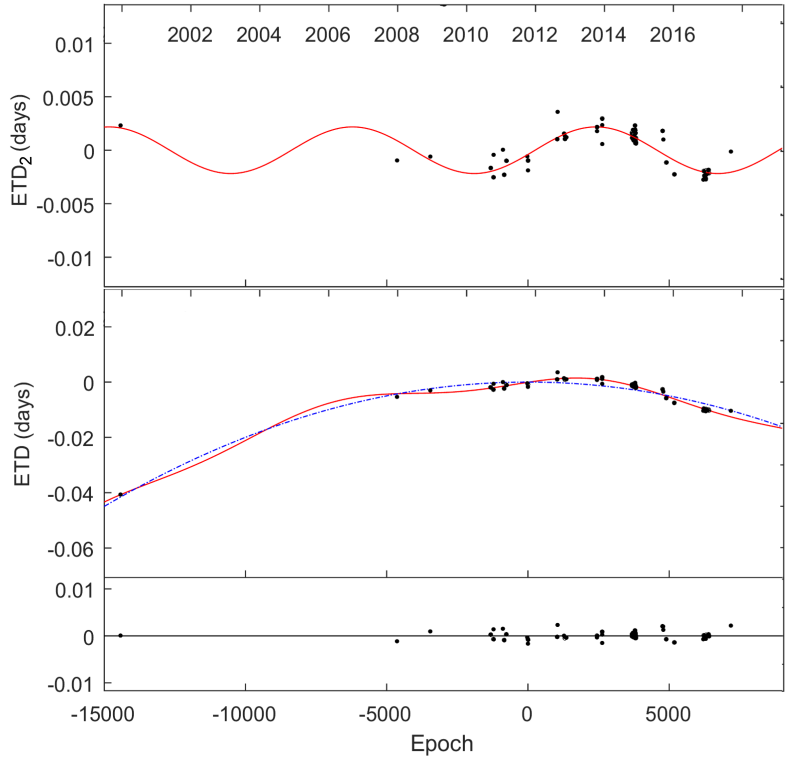

Fig. 4. SIMPLEX (Zasche *et al.* 2009) fit of eclipse timing differences for BN Ari between 1999 and 2017. *Top panel* illustrates simple sine curve fit ($e = 0$) of the quadratic residuals (ETD_2), the *middle panel* includes the quadratic and sine curve fits while the *bottom panel* shows the residuals ($\mathrm{SSR} = 0.0000402$) remaining after modeling.

Ignoring the last term ($\tau = 0$) for the moment, this initial rudimentary analysis (scaled Levenberg-Marquardt algorithm) leads to the following quadratic ephemeris for primary minimum:

$$\mathrm{HJD(MinI)} = 2\,451\,525.6685(15) + 0.2993776(1)\,E - 2.22(7) \times 10^{-10} E^2\,. \quad (3)$$

Since the quadratic coefficient (c_2) is less than zero, according to Eq.(4):

$$\mathrm{d}P/\mathrm{d}t = 2(365.24) \times c_2/P\,, \quad (4)$$

we initially propose that the orbital period is decreasing at a constant rate approaching 0.0468(16) s/y since 1999. The secular or long-term period change associated with an eclipse timing diagram described by a parabola is often attributed to mass transfer or by angular momentum loss due to magnetic stellar wind. Ideally when angular momentum loss dominates the net effect is a decreasing orbital period whereas the opposite is observed with conservative mass transfer from the secondary to the primary star. Interestingly we find another potential orbital period change which appears to be cyclic in nature embedded in the residuals remaining

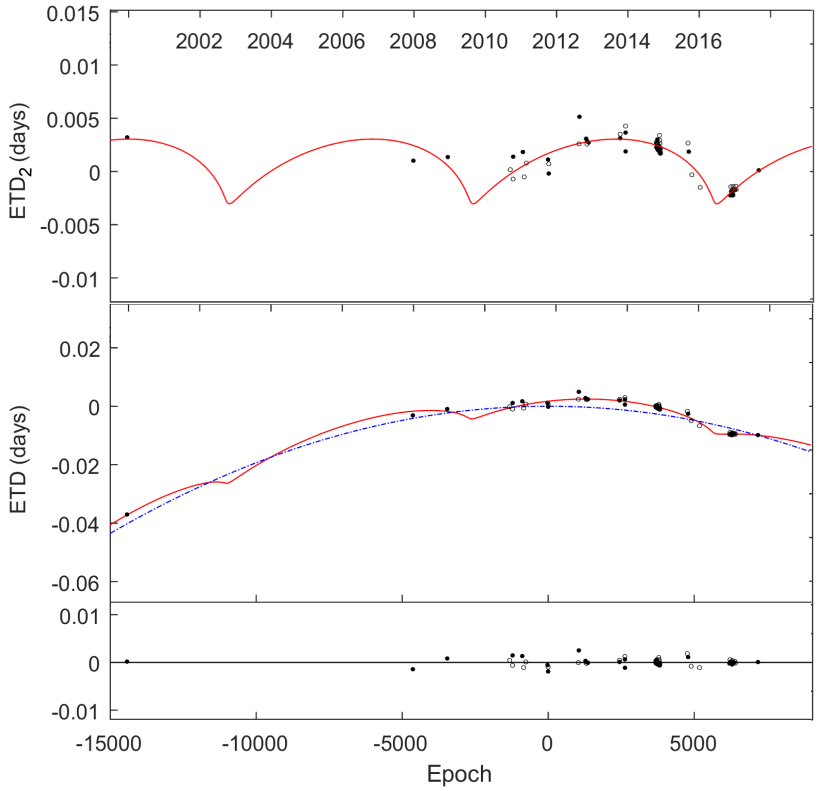

Fig. 5. SIMPLEX (Zasche *et al.* 2009) fit of eclipse timing differences for BN Ari between 1999 and 2017. *Top panel* illustrates LITE curve fit ($e = 0.83$) of the quadratic residuals (ETD$_2$), the *middle panel* includes the quadratic and LITE fits while the *bottom panel* shows the residuals (SSR = 0.0000352) remaining after modeling.

after the initial quadratic fit (Figs. 4 and 5). As long as this residual periodic wave appears symmetrical as shown in the top panel of Fig. 4, this behavior can be fit in its simplest form using a sine term:

$$\tau = c_3 \sin(c_4 E + c_5) \tag{5}$$

E is cycle number, and τ is time difference due to orbital motion. This preliminary Light-Time Effect (LITE) analysis assumes that the putative third body revolves about a common gravitational center in a circular orbit ($e = 0$). The amplitude of the oscillation, as defined by the coefficient of the sine term (c_3), was determined to be 0.00226 ± 0.00017 d while the period of the sinusoidal oscillations ($P_3 = 7.44 \pm 0.43$ yr) was calculated according to Eq.(6):

$$P_3 = 2\pi P/\omega \tag{6}$$

where ω (0.000692 ± 0.000040), the angular frequency, is defined by the coefficient c_4 and P is the orbital period of the binary pair in days. Cyclic changes of

eclipse timings may result from the gravitational influence of unseen companion(s) and/or periodic changes in the magnetic activity of either binary constituent. It has been known for at least a decade that a significant percent ($59 \pm 8\%$) of contact binaries exist as multiple systems (Pribulla and Ruciński 2006). The apparent sinusoidal-like behavior uncovered by ETD analysis is largely supported by data collected over the past decade which is only slightly longer than the proposed P_3 periodicity. Therefore, some caution should be exercised not to over-interpret these results. Nonetheless a more robust analysis was performed using the MATLAB code reported by Zasche *et al.* (2009) in which the associated parameters in the LITE equation (Irwin 1959) were derived by simplex optimization. These include P_3 (orbital period of star 3 and the 1–2 pair about their common center of mass), orbital eccentricity e, argument of periastron ω, time of periastron passage T_0 and amplitude $A = a_{12} \sin i_3$ (where a_{12} is semimajor axis of the 1–2 pair's orbit about the center of mass of the three-star system, and i_3 is orbital inclination of the third body in a three-star system). For the sake of simplicity, we initially calculated a minimum mass for the putative third body after assuming a circular orbit ($e = 0$) which is co-planar ($i_3 = 90^\circ$) with the binary pair. These results summarized in Table 4 and illustrated in Fig. 4, suggest the presence of a late M spectral type red dwarf with a mass ≈ 0.14 $M_\odot$. An object with this small mass would only provide a slight excess in luminosity ($L_3 < 0.2\%$). It is unlikely that this would result in a third light (l_3) value that was significantly different from zero during Roche modeling of the light curves (Section 3.6). However, if the orbital inclination is much shallower ($i_3 \approx 30^\circ$) the fractional luminosity (1.5%) of a third body with a minimum mass of about 0.3 $M_\odot$ could lead to third light parameter (l_3) values during Roche modeling that are statistically significant. The results (Table 4, Fig. 5) with the lowest residual sum of squares (SSR) indicate that a third body orbiting elliptically ($e = 0.83 \pm 0.05$) every 6.84 ± 0.16 yr with an inclination less than 45° would have sufficient minimum mass and added luminosity ($> 2.4\%$) to require correction (l_3) for a best fit Roche model. Both solutions ($e = 0$ or $e = 0.83$) are equally probable. However, if one were to steadfastly make a case for another gravitationally bound stellar object, there is a higher likelihood of observing the effect (l_3) with an elliptical orbit rather than a circular one. Before getting too far ahead with this third-light scenario for BN Ari, we need to address an alternate hypothesis for the sinusoidal variations in the orbital period of the binary pair. In this case, the mechanism for the underlying periodicity is probably not due to magnetic activity cycles attributed to Applegate (1992). According to an empirical relationship (Eq. 7, Lanza and Rodoǹo 1999) between the length of orbital period modulation and angular velocity ($\omega = 2\pi/P_{\rm orb}$):

$$\log P_{\rm mod} = 0.018 - 0.36 \log(2\pi/P_{\rm orb}). \qquad (7)$$

(where $P_{\rm mod}$ is in years and $P_{\rm orb}$ in seconds) any period modulation resulting from a change in the gravitational quadrupole moment would probably be closer to 21 yr

for BN Ari, not the much shorter periods ($P_3 \approx 6.8-7.4$ yr) estimated from the LITE analyses. Finally, a near-term linear ephemeris for primary minimum (Eq. 8) from the present investigation was projected from a straight line segment (Fig. 2 inset) covering observations from 2016 to 2017:

$$\mathrm{HJD(MinI)} = 2\,457\,994.5164(61) + 0.29937107(3)\,E\,. \qquad (8)$$

T a b l e 4

Putative period change, mass loss and third-body solution to the light-time effect (LITE) observed from changes in BN Ari eclipse timings

Parameter	Quadratic + Sine Term	LITE
HJD_0	2455843.8434 (3)	2455843.8418 (5)
T_0	–	2455043 (94)
P_3 [y]	7.61 (17)	6.84 (16)
A (semi-amplitude) [d]	0.00228 (56)	0.00304 (14)
ω [°]	–	238 (12)
e_3	0	0.83 (5)
$a_{12}\sin i$ [a.u.]	0.395 (97)	0.587 (28)
f(M_3)(mass function) [$\mathrm{M}_\odot$]	0.00107 (24)	0.00434 (3)
M_3 ($i = 90°$) [$\mathrm{M}_\odot$]	0.139 (12)	0.230 (6)
M_3 ($i = 60°$) [$\mathrm{M}_\odot$]	0.162 (12)	0.269 (7)
M_3 ($i = 45°$) [$\mathrm{M}_\odot$]	0.201 (16)	0.338 (9)
M_3 ($i = 30°$) [$\mathrm{M}_\odot$]	0.295 (24)	0.509 (14)
c_2 (quadratic coeff.) [10^{-10}]	$-1.991(1)$	$-1.935(1)$
$\mathrm{d}P/\mathrm{d}t$ [10^{-7} d/y]	$-4.878(2)$	$-4.721(2)$
$\mathrm{d}m_1/\mathrm{d}t$ [10^{-7} $\mathrm{M}_\odot$/y]	$-3.66(37)$	$-3.55(36)$
Sum of squared residuals	0.0000402	0.0000352

In order to maintain accurate ephemerides for this system, additional eclipse timings will be needed well into the foreseeable future.

3.3. Light Curve Behavior

Like all other W UMa-type eclipsing binary stars, BN Ari exhibits minima which are separated by 0.5 phase resulting from tidally locked rotation in a circular orbit (Fig. 1). No remarkable difference in brightness between Max I and Max II was observed during the UO and MAO campaigns. By contrast, photometric data (*V*-flux) taken between 2002 and 2009 (ASAS, Pojmański *et al.* 2005) showed considerable variability during minimum and maximum light (Fig. 6), a behavior characteristic of an active photosphere and often attributed to the presence of cool starspot(s) and/or hot region(s) which distort surface homogeneity (Yakut and Eggleton 2005).

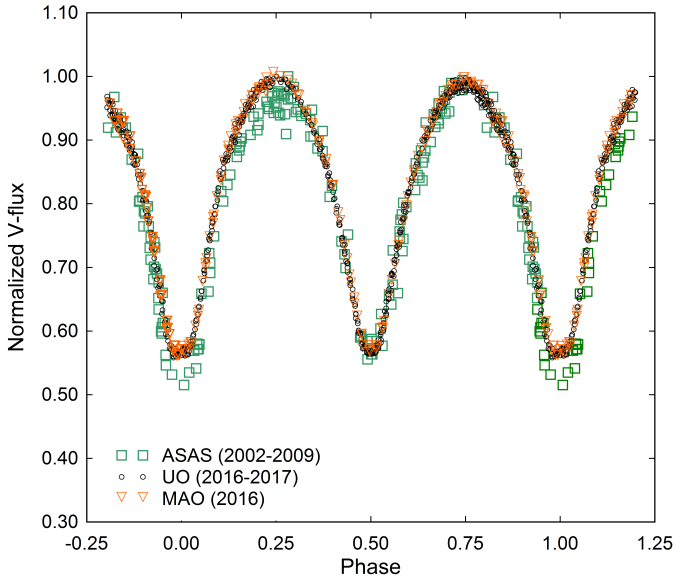

Fig. 6. Normalized *V*-flux data from BN Ari acquired by the ASAS survey between 2002 and 2009 ($P = 0.299374 \pm 0.000006$ d) superimposed with light curve results from UO (2016–2017) and MAO (2016). Variability at Min I and Max I are noteworthy suggesting an active photosphere.

3.4. Spectral Classification

Corrected and calibrated spectra of BN Ari recorded at West Challow Observatory were combined to yield a 1D spectral profile for each night and then visually compared to spectra from the Pickles Stellar Spectral Flux Library (Pickles 1998). The best visual match (Fig. 7) of the BN Ari spectrum was to spectral type K1V (mean of K0V and K2V). The conclusion that K1V was the most likely spectral type of BN Ari was confirmed by analytically fitting its profile to spectral types from K0V to K3V. Also, given the relatively small contribution ($< 2\%$) in overall luminosity from third light, it is unlikely that a nearby dim ($V \approx 16.5$ mag) spectral class M star would significantly affect the final outcome. Based on these findings an effective temperature of 5170 K was adopted for the secondary, which throughout this paper is considered the more massive star.

3.5. Radial Velocity

A log of all spectra captured from September 14, 2016 to September 12, 2017 at DAO is provided in Table 5 while two sample spectra are illustrated in Fig. 8. Spectral reduction was performed using the application RAVERE (see footnote 1). Final extraction of the RV data employed broadening functions (BROAD – see footnote 1) to improve peak resolution. Further details regarding the advantages of using wavelength broadening functions for contact binary systems are described by Ruciński (2004).

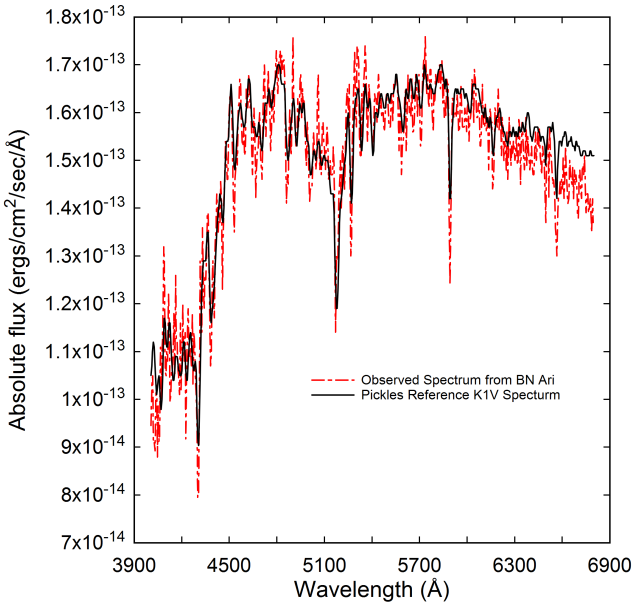

Fig. 7. Pickles reference spectrum for K1V star superimposed on observed spectrum for BN Ari.

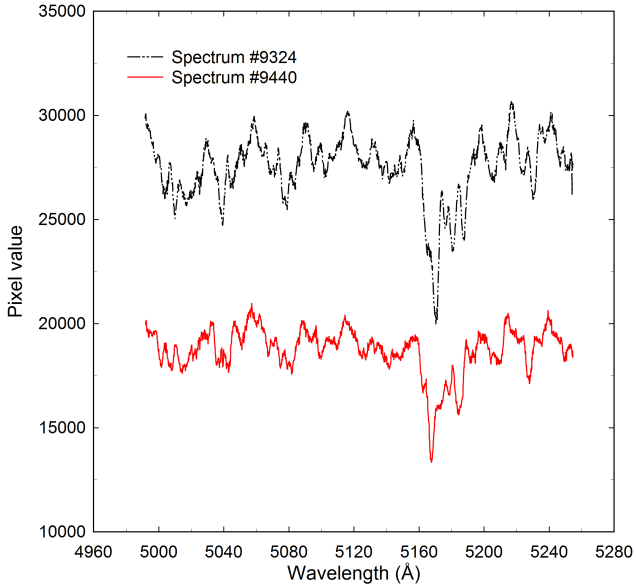

Fig. 8. Spectra from files 9324 (*upper*) and 9440 (*lower*) at phases 0.769 and 0.227 respectively. Note the strong neutral iron lines (at 5167.487 Å and 5171.595 Å) and the strong neutral magnesium triplet (at 5167.33 Å, 5172.68 Å, and 5183.61 Å).

3.6. Roche Modeling Approach

The RV data reported herein (Table 5) for the first time were essential to obtaining a definitive solution for the total mass, the mass ratio (m_2/m_1) and confirming that BN Ari is a W-type contact binary system. In this case the hotter,

T a b l e 5

Log of 17 spectral observations taken at the DAO between September 14, 2016 and September 12, 2017

DAO Image#	Mid-time HJD-2400000	Exposure [s]	Phase at Mid-exp	V_1 [km/s]	V_1 Err	V_2 [km/s]	V_2 Err
9324	57645.9734	2000	0.769	232.01	5.8	−135.76	7.3
9440	57650.0171	2000	0.277	−289.97	4.1	59.82	13.5
9442	57650.0412	2000	0.357	−243.54	3.5	34.99	4.3
9484	57652.8435	1200	0.719	215.81	5.5	−135.26	3.6
9486	57652.8596	1200	0.772	224.66	6.9	−128.32	4.6
9507	57652.9876	900	0.200	−274.32	3.1	71.45	10.9
9509	57653.0005	900	0.243	−286.41	3.1	71.01	13.6
9511	57653.0105	1200	0.277	−284.79	2.6	60.07	11.6
9513	57653.0303	1200	0.343	−259.09	3.1	44.09	6.2
9517	57653.0528	935	0.418	–	–	27.5	4.9
9606	57654.0375	1200	0.707	212.91	6.1	−135.16	3.6
9608	57654.0494	800	0.747	223.69	6.2	−133.20	5.3
15710	57997.8748	1800	0.229	−305.47	5.7	64.91	14.3
15817	57999.9852	1800	0.278	−302.13	3.9	66.75	11.6
1595	58007.8763	1800	0.639	153.51	3.7	−126.7	5.7
15911	58007.9225	1500	0.794	224.82	6.6	−141.32	6.3
15953	58008.8311	1800	0.829	202.82	6.6	−133.79	5.8

but less massive star (herein defined as the primary) is eclipsed by its cooler and more massive stellar partner. Modeling of light curve of data from BN Ari was primarily accomplished using the programs PHOEBE 0.31A (Prŝa and Zwitter 2005) and WDWINT56A (see footnote 1) both of which provide an interface to the Wilson-Devinney (W-D) code (Wilson and Devinney 1971, Wilson 1979, Wilson 1990). WDWINT56A makes use of Kurucz's atmosphere models (Kurucz 2002) which are integrated over $UBVR_JI_JR_cI_c$ and *ubvy* optical passbands. The model selected was for an overcontact binary (Mode 3). Bolometric albedo ($A_{1,2} = 0.5$) and gravity darkening coefficients ($g_{1,2} = 0.32$) for cooler stars (< 7500 K) with convective envelopes were respectively assigned according to Ruciński (1969) and Lucy (1967). Following any change in the effective temperature ($T_{\rm eff_1}$) of the primary star, new logarithmic limb darkening coefficients (x_1, x_2, y_1, y_2) were interpolated according to van Hamme (1993). The effective temperature of the cooler, albeit more luminous star was fixed ($T_{\rm eff_2} = 5170$ K) in accordance with the earlier assignment of BN Ari as spectral type K1V. Subsequently, RV and light curve data were simultaneously modeled using WDWINT56A in order to obtain the best estimates for mass ratio (q), the semi-major axis of the binary system, and the systemic velocity (V_γ). Initially, direct least-squares curve fitting of the RV data alone was carried out in an Excel spreadsheet developed by R.H.N. which uses the Solver add-in utility. These results indicated that $q = 2.543 \pm 0.058$, $V_\gamma = -35.7 \pm 1.3$ km/s, $M_1 = 0.44$ M$_\odot$, $M_2 = 1.11$ M$_\odot$, $V_1 = -261.5 \pm 1.5$ km/s

and $V_2 = 102.8 \pm 2.4$ km/s. Initially during W-D modeling, all but the temperature of the more massive star ($T_{\rm eff_2}$), orbital period ($P = 0.299371$ d), bolometric albedo ($A_{1,2} = 0.5$) and gravity darkening coefficients ($g_{1,2} = 0.32$) were allowed to vary during W-D DC program iterations. In general, the best fits for $T_{\rm eff_1}$, i, and Roche potentials ($\Omega_1 = \Omega_2$) were collectively established (method of multiple subsets) by DC before exploring simultaneous changes to i, $T_{\rm eff_1}$, q, $\Omega_{1,2}$, V_γ and the semi-major axis. Once the Roche model fit was optimized using the monochromatic (V-flux) light curve, the other light curves (B and I_c) were added to the model. Thereafter, $T_{\rm eff_2}$ remained fixed, while simultaneously varying $T_{\rm eff_1}$, i, q, V_γ, semi-major axis and the Roche potential ($\Omega_1 = \Omega_2$) until the model converged to a best fit. Since there did not appear significant differences in brightness during quadrature, Roche modeling initially proceeded without the incorporation of spots. However, in view of the underlying sinusoidal-like variations observed in the eclipse timing residuals, the third light parameter (l_3) was also allowed to freely vary during DC. Modeling of light curve data from MAO (V, R_c and I_c) and those (B and V only) published by Michaels (2015) were analyzed in a similar fashion.

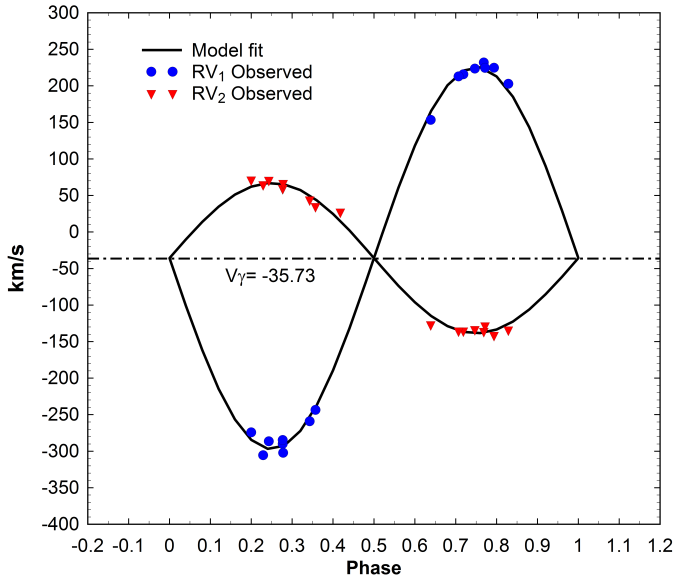

Fig. 9. Radial velocity profile following simultaneous fit with light curve data using the W-D code (WDWINT56A).

3.7. Roche Modeling Results

Importantly, simultaneous Roche modeling of RV and light curve (V) data clearly demonstrates that BN Ari is a W-type overcontact system (Figs. 1, 2, and 10). Initial attempts to obtain an acceptable fit for the light curves fell short due to the model overshooting the observed data at minimum light. This was particu-

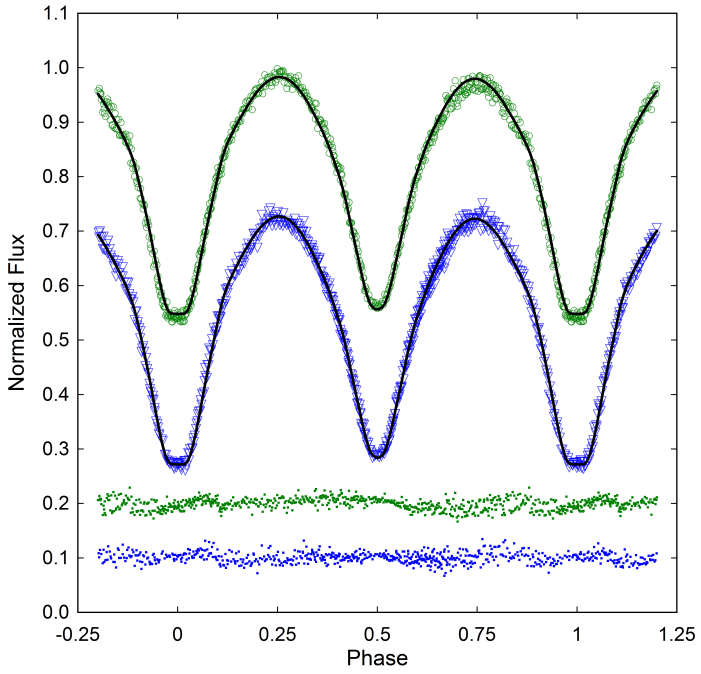

Fig. 10. Period folded CCD light curves for BN Ari produced from photometric data (Michaels 2015) obtained in 2014. The *top* (*V*) and *bottom* curve (*B*) were reduced to normalized flux. Synthetic fits (solid-line) from Roche modeling assumed a W-type W UMa binary with a single hot spot. Flux and residuals from the model fits are offset for clarity.

larly notable with the R_c- and I_c-bandpass curves but was successfully addressed by invoking third light (l_3) into the Roche model. This phenomenon could result from simple light contamination by an unresolved background star. However, the likelihood of a gravitationally bound body is supported by the eclipse-timing period analysis (Section 3.2) which suggested that BN Ari was a triple system with a mid-to-late M-class star orbiting ($P_3 \approx 6.8$ yr) the common center of mass. The light curve parameters and geometric elements determined for each of these model fits are summarized in Table 6 (unspotted) and Table 7 (spotted). It is important to note that the listed errors are improbably low and only reflect the model fit to the observations which assumed exact values for all fixed parameters. In all likelihood, the true errors are many fold higher. Spatial models ($\phi = 0.15$) of the Roche surface (Fig. 11) rendered with BM3 using the physical and geometric elements derived from the UO, MAO and Michaels (2015) light curves, suggest that during recent epochs a hot spot on the less massive star has persisted near the neck region.

The fill-out parameter (f) which corresponds to a volume percent of the outer surface shared between each star was calculated (Eq. 9) according to Kallrath and Milone (1999) and Bradstreet (2005) where:

$$f = (\Omega_{\rm inner} - \Omega_{1,2})/(\Omega_{\rm inner} - \Omega_{\rm outer})\,. \qquad (9)$$

T a b l e 6

Synthetic light curve parameters employed for Roche modeling (unspotted) and the values derived from simultaneous modeling of light curve and RV data from BN Ari

Parameter[a]	UO 2016-2017	MAO 2016	Michaels (2015)	Michaels + RV
$T_{\rm eff_1}^{\rm (b)}$ [K]	5282 ± 2	5251 ± 6	5731 ± 2	5351 ± 3
$T_{\rm eff_1}^{\rm (a)}$ [K]	5170	5170	5527	5170
$q^{\rm (b)}$	2.548 ± 0.001	2.555 ± 0.014	2.699 ± 0.004	2.578 ± 0.007
$A^{\rm (a)}$	0.5	0.5	0.5	0.5
$g^{\rm (a)}$	0.32	0.32	0.32	0.32
$\Omega_1 = \Omega_2^{\rm (b)}$	5.942 ± 0.006	5.941 ± 0.018	6.120 ± 0.006	5.947 ± 0.010
$i^{\circ})^{\rm (b)}$	83.79 ± 0.19	84.11 ± 0.98	85.06 ± 0.23	83.87 ± 0.24
$L_1/(L_1+L_2)_B^{\rm (b,c)}$	0.3312 ± 0.0002	–	0.3449 ± 0.0005	0.3497 ± 0.0001
$L_1/(L_1+L_2)_V^{\rm (b,c)}$	0.3239 ± 0.0002	0.3177 ± 0.0007	0.3314 ± 0.0004	0.3376 ± 0.0002
$L_1/(L_1+L_2)_{Rc}^{\rm (b,c)}$	–	0.3144 ± 0.0007	–	–
$L_1/(L_1+L_2)_{Ic}^{\rm (b,c)}$	0.3169 ± 0.0001	0.3123 ± 0.0008	–	–
$L_3/(L_1+L_2+L_3)_B^{\rm (b,d)}$	$0.172 \pm 0.001\%$	–	–	$0.177 \pm 0.003\%$
$L_3/(L_1+L_2+L_3)_V^{\rm (b,d)}$	$0.107 \pm 0.001\%$	$0.204 \pm 0.016\%$	–	$0.193 \pm 0.003\%$
$L_3/(L_1+L_2+L_3)_{Rc}^{\rm (b,d)}$	–	$0.291 \pm 0.016\%$	–	–
$L_3/(L_1+L_2+L_3)_{Ic}^{\rm (b,d)}$	$0.324 \pm 0.001\%$	$0.383 \pm 0.018\%$	–	–
r_1(pole)$^{\rm (b)}$	0.2864 ± 0.0003	0.2870 ± 0.0010	–	0.2882 ± 0.0004
r_1(side)	0.2992 ± 0.0003	0.3000 ± 0.0012	–	0.3015 ± 0.0004
r_1(back)	0.3357 ± 0.0005	0.3371 ± 0.0021	–	0.3401 ± 0.0007
r_2(pole)$^{\rm (b)}$	0.4393 ± 0.0006	0.4403 ± 0.0016	–	0.4428 ± 0.0009
r_2(side)	0.4703 ± 0.0008	0.4715 ± 0.0022	–	0.4748 ± 0.0012
r_2(back)	0.4988 ± 0.0010	0.5004 ± 0.0030	–	0.5042 ± 0.0017
Fill-out factor f	6.2%	7.1%	15%	9.1%
rms (B)$^{\rm (e)}$	0.005	–	0.005	0.005
rms (V)$^{\rm (e)}$	0.088	0.008	0.011	0.012
rms (R_c)$^{\rm (e)}$	–	0.008	–	–
rms (I_c)$^{\rm (e)}$	0.018	0.008	–	–

(a) Fixed during DC, (b) Error estimates for q, i, Ω_1, Ω_2 and $T_{\rm eff_1}$, $L_1/(L_1+L_2)$, $L_3/(L_1+L_2+L_3)$, r_1 and r_2 (pole, side and back) from WDWINT56A (see footnote 1), (c) Bandpass dependent fractional luminosity, L_1 and L_2, refer to luminosities of the primary and secondary stars, respectively, (d) Third light (L_3 = % luminosity at $\phi = 0.25$), (e) Monochromatic root mean square (*rms*) of residuals from best Roche model fits.

In general the light curve modeling results reported here are in agreement with those obtained by Michaels (2015) with two notable exceptions. Differences (5527 K *vs.* 5170 K) in the effective temperature of the more massive star arise from differences in the adopted spectral type (G7V *vs.* K1V), the latter of which is based on our definitive classification spectrum. Secondly, our light curves were best fit after invoking the third light parameter (l_3) and did not require adding a cool spot to the model (Table 7).

T a b l e 7

Synthetic light curve parameters employed for Roche modeling (spotted) and the values derived from simultaneous modeling of light curve and RV data from BN Ari

Parameter[a]	UO 2016-2017	MAO 2016	Michaels (2015)	Michaels + RV
$T_{\rm eff_1}^{(a)}$ [K]	5278 ± 2	5262 ± 3	5728 ± 3	5341 ± 3
$T_{\rm eff_1}^{(b)}$ [K]	5170	5170	5527	5170
$q^{(b)}$	2.554 ± 0.004	2.530 ± 0.001	2.685 ± 0.002	2.566 ± 0.001
$A^{(a)}$	0.5	0.5	0.5	0.5
$g^{(a)}$	0.32	0.32	0.32	0.32
$\Omega_1 = \Omega_2^{(b)}$	5.942 ± 0.005	5.942 ± 0.005	6.114 ± 0.004	5.926 ± 0.010
$i^{\circ\,(b)}$	83.52 ± 0.17	82.74 ± 0.18	82.23 ± 0.10	83.61 ± 0.21
$A = T_{\rm spot}/T_p^{(b)}$	1.095 ± 0.002	1.075 ± 0.003	1.11 ± 0.050	1.110 ± 0.012
θ_p (co-latitude)$^{(b)}$	96 ± 2	73.5 ± 6	92 ± 19	101.9 ± 6
φ_p (longitude)$^{(b)}$	355 ± 1	349 ± 1	9 ± 8	351.8 ± 2
r_p (angular radius)$^{(b)}$	25.4 ± 0.2	26.5 ± 0.5	15 ± 6	13.9 ± 0.6
$A = T_{\rm spot}/T_s^{(b)}$	–	–	0.95 ± 0.06	–
θ_s (co-latitude)$^{(b)}$	–	–	39 ± 9	–
φ_s (longitude)$^{(b)}$	–	–	299 ± 4	–
r_s (angular radius)$^{(b)}$	–	–	18 ± 9	–
$L_1/(L_1+L_2)_B^{(b,c)}$	0.3302 ± 0.0002	–	0.3454 ± 0.0006	0.3482 ± 0.0001
$L_1/(L_1+L_2)_V^{(b,c)}$	0.3231 ± 0.0001	0.3219 ± 0.0002	0.3312 ± 0.0004	0.3368 ± 0.0002
$L_1/(L_1+L_2)_{Rc}^{(b,c)}$	–	0.3183 ± 0.0002	–	–
$L_1/(L_1+L_2)_{Ic}^{(b,c)}$	0.3161 ± 0.0001	0.3159 ± 0.0002	–	–
$L_3/(L_1+L_2+L_3)_B^{(b,d)}$	$0.273 \pm 0.004\%$	–	–	$0.169 \pm 0.003\%$
$L_3/(L_1+L_2+L_3)_V^{(b,d)}$	$0.224 \pm 0.003\%$	$0.173 \pm 0.004\%$	–	$0.289 \pm 0.003\%$
$L_3/(L_1+L_2+L_3)_{Rc}^{(b,d)}$	–	$0.341 \pm 0.005\%$	–	–
$L_3/(L_1+L_2+L_3)_{Ic}^{(b,d)}$	$0.428 \pm 0.003\%$	$0.398 \pm 0.005\%$	–	–
r_1(pole)$^{(b)}$	0.2868 ± 0.0002	0.2885 ± 0.0004	–	0.2890 ± 0.0003
r_1(side)	0.2998 ± 0.0002	0.3017 ± 0.0005	–	0.3025 ± 0.0004
r_1(back)	0.3368 ± 0.0004	0.3393 ± 0.0008	–	0.3415 ± 0.0006
r_2(pole)$^{(b)}$	0.4401 ± 0.0005	0.4402 ± 0.0007	–	0.4429 ± 0.0010
r_2(side)	0.4713 ± 0.0006	0.4715 ± 0.0009	–	0.4749 ± 0.0013
r_2(back)	0.5000 ± 0.0009	0.5007 ± 0.0013	–	0.5046 ± 0.0018
Fill-out factor f	6.9%	6.9%	13%	9.6%
rms (B)$^{(e)}$	0.004	–	0.005	0.005
rms (V)$^{(e)}$	0.008	0.006	0.010	0.011
rms (R_c)$^{(e)}$	–	0.007	–	–
rms (I_c)$^{(e)}$	0.016	0.007	–	–

(a) Fixed during DC, (b) Error estimates for q, i, Ω_1, Ω_2 and $T_{\rm eff_1}$, $L_1/(L_1+L_2)$, $L_3/(L_1+L_2+L_3)$, spot parameters (A, θ, φ, r), r_1 and r_2 (pole, side and back) from WDwint56a (see footonote 1), (c) Bandpass dependent fractional luminosity, L_1 and L_2, refer to luminosities of the primary and secondary stars, respectively, (d) Third light (L_3 = % luminosity at $\phi = 0.25$), (e) Monochromatic root mean square (*rms*) of residuals from best Roche model fits.

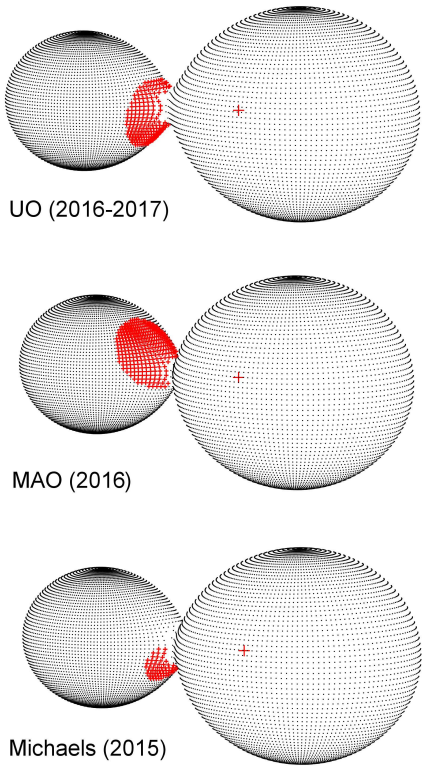

Fig. 11. Spatial models at $\phi = 0.15$ showing the putative location of a hot spot on the secondary star during 2014 and from late 2016 to early 2017.

3.8. Absolute Parameter Estimates

Apart from a spectroscopic mass ratio ($q_{\rm sp}$), the other critical values provided by RV data are the orbital speeds ($v_{1r} + v_{2r}$). Importantly, the total mass can be calculated according to Eq.(10) when the orbital inclination (i) is known:

$$(m_1 + m_2)\sin^3 i = (P/2\pi G)(v_{1r} + v_{2r})^3 . \quad (10)$$

Average results from all the best fit models (single hot spot) reveal that $v_{1r} = 262.0 \pm 1.9$ km/s, $v_{2r} = 98.13 \pm 5.02$ km/s, $V_\gamma = -36.87 \pm 0.70$, and $i = 83.^\circ29 \pm 0.^\circ11$. The total mass of the system was determined to be 1.46 ± 0.07 M$_\odot$. Since $q = 2.55 \pm 0.01$ then the secondary mass is equal 1.054 ± 0.046 M$_\odot$ and primary mass is equal 0.413 ± 0.018 M$_\odot$. The semi-major axis, $a = 2.14 \pm 0.04$ R$_\odot$, was calculated from the Kepler's third law:

$$a^3 = GP^2(M_1 + M_2)/4\pi^2. \quad (11)$$

These values were used for subsequent determinations of the binary volume-radius r_L, bolometric magnitude $M_{\rm bol}$ and distance d [pc] to BN Ari. The effective

radius of each Roche lobe can be calculated using Eq.(12) derived by Eggleton (1983) which only requires a value for the mass ratio:

$$r_L = \left(0.49q^{2/3}\right) / \left(0.6q^{2/3} + \ln(1+q^{1/3})\right) \quad (12)$$

where values for r_1 (0.3015 ± 0.0001) and r_2 (0.4616 ± 0.0001) were respectively determined for the primary and secondary stars. One can calculate the solar radii for both binary constituents where $R_1 = a \times r_1 = (0.645 \pm 0.011$ R$_\odot$) and $R_2 = a \times r_2 = (0.988 \pm 0.016$ R$_\odot$) since the semi-major axis and the volume radii are known. The bolometric magnitudes ($M_{\rm bol1,2}$) and luminosity in solar units (L$_\odot$) for the primary (L_1) and secondary stars (L_2) were calculated from well known relationships where:

$$M_{\rm bol1,2} = 4.75 - 5\log(R_{1,2}/{\rm R}_\odot) - 10\log(T_{1,2}/T_\odot) \quad (13)$$

and

$$L_{1,2} = (R_{1,2}/{\rm R}_\odot)^2 \times (T_{1,2}/T_\odot)^4. \quad (14)$$

T a b l e 8

Absolute parameters for BN Ari using results from Roche modeling of the 2014 (Michaels 2015), 2016 (MAO) and 2016–2017 (UO) light curves

Parameter	Primary	Secondary
Mass [M$_\odot$]	0.413 ± 0.018	1.054 ± 0.046
Radius [R$_\odot$]	0.645 ± 0.011	0.988 ± 0.016
a [R$_\odot$]	2.14 ± 0.04	–
Luminosity [L$_\odot$]	0.268 ± 0.009	0.690 ± 0.023
$M_{\rm bol}$	6.10 ± 0.07	5.27 ± 0.07
$\log g$	4.435 ± 0.024	4.471 ± 0.024

Absolute parameters (Table 8) were derived for each star in this W-type W UMa binary system using results from the best fit (spotted) simulations. Since high precision light curve data independently produced at three different observatories were available, mean estimates for mass [M$_\odot$], radius [R$_\odot$], semi-major axis [R$_\odot$], luminosity [L$_\odot$] and $\log(g)$ were calculated from the best fit data. Assuming that $T_{\rm eff_1} = 5294 \pm 42$ K, $T_{\rm eff_2} = 5170$ K, and $T_\odot = 5772$ K, then the solar luminosities for the primary and secondary are $L_1 = 0.268 \pm 0.009$ L$_\odot$ and $L_2 = 0.690 \pm 0.023$ L$_\odot$, respectively.

3.9. Distance to BN Ari

Using V data from UO, bolometric magnitudes were calculated to be $M_{\rm bol2} = 5.16 \pm 0.06$ mag and $M_{\rm bol1} = 6.18 \pm 0.06$ mag. Combining the bolometric magnitudes resulted in $M_{\rm bol1,2} = 4.81 \pm 0.08$ mag and when adjusted with the bolometric

correction ($BC = -0.259$ mag) interpolated from Pecaut and Mamajek (2013) the absolute magnitude (M_v) was determined to be 5.07 ± 0.08 mag. The distance modulus:

$$d\ [\mathrm{pc}] = 10^{((m-M_v)-A_v+5)/5))} \tag{15}$$

where $m = V_{\mathrm{max}}$ (10.30 ± 0.01 mag) and $A_v = 0.02$ mag (determined according to Amôres and Lépine (2005)) leads to an estimated distance of 110 ± 4 pc to BN Ari. This is lower than that (123.2 ± 0.74 pc) calculated directly from parallax data (8.1158 ± 0.0488 mas) recently included in the Gaia DR-2 release (Prusti *et al.* 2016, Brown *et al.* 2018). Assuming that the Gaia DR2 parallax data are the gold standard from which distances can be determined, we suspect that either our V_{max} value is too bright and/or interstellar extinction (A_v) is negligible in this region of the sky. Parenthetically, had V_{avg} (10.53 ± 0.22 mag) rather than V_{max} (10.30 ± 0.01 mag) been used, the distance estimate (124 ± 13 pc) would have been much closer to the parallax value, albeit more variable. The reader should also be reminded that the BVI_c magnitudes determined in this study are catalog-based (MPOSC3) using ensemble photometry and not derived using a standard starfield. For the sake of comparison, the distance to BN Ari was also estimated using an empirical relationship derived from a calibrated model specifically for contact binaries. Luminosity calibration from a subset of contact binaries based upon orbital period ($0.275 < P < 0.575$ d) and the Tycho-Gaia Astrometric Solution parallax data (Mateo and Ruciński 2017) showed that the absolute magnitude (M_V) can be estimated using Eq.(16):

$$M_V = (-8.67 \pm 0.65)(\log P + 0.4) + (3.73 \pm 0.06). \tag{16}$$

According to this relationship the absolute magnitude was calculated to be $M_V = 4.80 \pm 0.10$ mag so that substitution back into Eq.(15) yields a distance of 124 ± 6 pc. The median ($\pm$ mean absolute deviation) distance to this system is therefore estimated to be 123.2 ± 2.4 pc.

4. Conclusions

CCD-based photometric data collected in *B, V,* R_c and I_c-bands produced 15 new times-of-minimum for BN Ari. The linear ephemeris for BN Ari was updated and potential changes in orbital periodicity assessed from the differences between the observed and predicted times-of-minimum calculated between 1999 and 2017. The ETD diagram for BN Ari produced a parabolic curve suggesting that since 1999 the orbital period has been decreasing at a rate of at least 0.041 ± 0.001 s/y. Furthermore, residuals from the best fit LITE modeling uncovered a sinusoidal-like variation in the orbital period that repeats every 6.84 ± 0.16 yr. This behavior is most probably associated with the light-time effect resulting from the gravitational influence of an elliptically orbiting red dwarf. Additional eclipse timings over the next decade could prove useful to confirm this finding and/or expose additional

sources of orbital period variability. Evidence from new spectral classification data indicates that the secondary but most luminous star is a K1V spectral type ($T_{\rm eff_2} \approx$ 5170 K) star. Radial velocity data reported for the first time herein led to a robust light curve solution using the W-D code. Armed with the necessary physical data (q, i and $T_{\rm eff_2}$) to constrain the Roche model, simulations confirm that BN Ari is a W-type W UMa variable. Even though maximum light at $\phi = 0.25$ and 0.75 had near equal intensity, a hot spot positioned near the neck region of the primary star achieved the best simultaneous multicolor fits. Nonetheless, addition of the third light parameter (l_3) was still necessary to obtain the best fit during minimum light.

Acknowledgements. This research has made use of the SIMBAD database, operated at Centre de Données astronomiques de Strasbourg, France. Time-of-minima data from the IBVS and VSOLJ websites proved invaluable to the assessment of period changes experienced by this variable star. In addition, the Northern Sky Variability Survey hosted by the Los Alamos National Laboratory and the International Variable Star Index maintained by the AAVSO were mined for valuable information. The diligence and dedication shown by all associated with these organizations is very much appreciated. This work has made use of data from the European Space Agency (ESA) mission Gaia (*https://www.cosmos.esa.int/gaia*), processed by the Gaia Data Processing and Analysis Consortium (DPAC). R.H.N. wishes to thank the staff members at the DAO (Dmitry Monin, David Bohlender, and the late Les Saddlmyer) for their usual splendid help and assistance. A special thank you to Prof. Petr Zasche who provided his MATLAB LITE code and valuable assistance in running the application. The authors are most thankful for the careful review and critical evaluation of this study by an anonymous referee.

REFERENCES

Alton, K.B. 2016, *JAAVSO*, **44**, 87.
Amôres, E.B., and Lépine, J.R.D. 2005, *AJ*, **130**, 659.
Applegate, J.H. 1992, *ApJ*, **385**, 621.
Bradstreet, D.H., and Steelman, D.P. 2002, *Bull. AAS*, **34**, 1224.
Bradstreet, D.H. 2005, *Society for Astronomical Sciences Annual Symposium*, **24**, 23.
Brown, A.G.A., *et al.* 2018, arXiv:1804.09365.
Diethelm, R. 2011, *IBVS*, 5960.
Diethelm, R. 2012, *IBVS*, 6011.
Eggleton, P.P. 1983, *ApJ*, **268**, 368.
Harris, A.W., *et al.* 1989, *Icarus*, **77**, 171.
Hoňková, K., *et al.* 2013, *Open European Journal on Variable stars*, 160.
Hübscher, J. 2014, *IBVS*, 6118.
Hübscher, J. 2015, *IBVS*, 6152.
Hübscher, J., and Lehmann, P.B. 2013, *IBVS*, 6070.
Irwin, J.B. 1959, *AJ*, **64**, 149.
Kallrath, J and Milone, E.F. 1999, in: "Eclipsing Binary Stars: Modeling and Analysis", Springer-New York.

Kwee, K.K., and Woerden, H. van 1956, *Bulletin of the Astronomical Institutes of the Netherlands*, **12**, 327.
Kurucz, R.L. 2002, *Baltic Astronomy*, **11**, 101.
Lanza, A.F., and Rodonò, M. 1999, *A&A*, **349**, 887.
Lucy, L.B. 1967, *Zeitschrift für Astrophysik*, **65**, 89.
Mateo, N.M., and Ruciński, S.M. 2017, *AJ*, **154**, 125.
Michaels, E.J. 2015, *JAAVSO*, **43**, 231.
Nagai, K. 2012, *VSOLJ Variable Star Bulletin*, **53**, 2.
Nagai, K. 2013, *VSOLJ Variable Star Bulletin*, **55**, 2.
Nagai, K. 2014, *VSOLJ Variable Star Bulletin*, **56**, 1.
Nagai, K. 2016, *VSOLJ Variable Star Bulletin*, **61**, 1.
Nelson, R.H. 2010, in: "Spectroscopy for Eclipsing Binary Analysis in The Alt-Az Initiative", Collins Foundation Press, Santa Margarita, CA, Eds. R.M. Genet, J.M. Johnson and V. Wallen.
Nelson, R.H. 2011, *IBVS*, 5966.
Nelson, R.H. 2012, *IBVS*, 6018.
Nelson, R.H. 2017, *IBVS*, 6195.
Otero, S.A, Wils, P., and Dubovsky, P.A. 2004, *IBVS*, 5570.
Paschke, A. 2009, *Open European Journal on Variable Stars*, 116.
Paschke, A. 2011, *Open European Journal on Variable Stars*, 142.
Paschke, A. 2013, *Open European Journal on Variable Stars*, 155.
Pecaut, M.J., and Mamajek, E.E. 2013, *ApJS*, **208**, 9.
Pickles, A.J. 1998, *PASP*, **110**, 863.
Pojmański, G., Pilecki, B., and Szczygiel, D. 2005, *Acta Astron.*, **55**, 275.
Pribulla, T., and Rucinski, S.M. 2006, *AJ*, **13**, 2986.
Prša, A., and Zwitter, T. 2005, *ApJ*, **628**, 426.
Prusti, T., *et al.* 2016, *A&A*, **595**, A1.
Ruciński, S.M. 1969, *Acta Astron.*, **19**, 245.
Ruciński, S.M. 2004, *IAU Symposium*, **215**, 17.
Samolyk, G. 2016, *JAAVSO*, **44**, 69.
Sánchez-Blázquez, P., *et al.* 2006, *MNRAS*, **371**, 703.
Schwarzenberg-Czerny, A. 1996, *ApJ*, **460**, L107.
van Hamme, W. 1993, *AJ*, **106**, 2096.
Warner, B.D. 2007, *Minor Planet Bulletin*, **34**, 113.
Wilson, R.E. 1979, *ApJ*, **234**, 1054.
Wilson, R.E. 1990, *ApJ*, **356**, 613.
Wilson, R.E., and Devinney, E.J. 1971, *ApJ*, **166**, 605.
Woźniak, P.R., *et al.* 2004, *AJ*, **127**, 2436.
Yakut, K., and Eggleton, P.P. 2005, *ApJ*, **629**, 1055.
Zasche, P., Liakos, A., Niarchos, P., Wolf, M., Manimanis, V., and Gazeas, K. 2009, *New Astronomy*, **14**, 121.